UC Berkeley
UC Berkeley Previously Published Works

Title

Biomechanics of aerial righting in wingless nymphal stick insects

Permalink

Journal

Interface Focus, 7(1)

ISSN

2042-8898

Authors

Zeng, Yu
Lam, Kenrick
Chen, Yuexiang
et al.

Publication Date

2017-02-06

DOI

10.1098/rsfs.2016.0075

Peer reviewed

Author for correspondence:
Yu Zeng
e-mail: dreavoniz@berkeley.edu

THE ROYAL SOCIETY
PUBLISHING

Biomechanics of aerial righting in wingless nymphal stick insects

Yu Zeng[1,2], Kenrick Lam[1], Yuexiang Chen[1], Mengsha Gong[1], Zheyuan Xu[1] and Robert Dudley[1,3]

[1]Department of Integrative Biology, University of California, Berkeley, CA 94720, USA
[2]Department of Physics, University of California, Merced, CA, USA
[3]Smithsonian Tropical Research Institute, Balboa, Republic of Panama

YZ, 0000-0002-2651-227X

Numerous wingless arthropods as well as diverse vertebrates are capable of mid-air righting. We studied the biomechanics of the aerial righting reflex in first-instar nymphs of the stick insect *Extatosoma tiaratum*. After being released upside-down, insects reoriented dorsoventrally and stabilized body posture via active modulation of limb positions and associated aerodynamic torques. We identified specific reflexes for bilaterally asymmetric leg displacements which elicit body rotation and subsequently stabilize mid-air posture. Coordinated appendicular movements thus improve torsional manoeuvrability in the absence of wings, as may have characterized the initial origins of controlled aerial behaviour in arthropods. Design of small aerial or multimodal robotic vehicles may similarly benefit from use of such strategies for flight control.

1. Introduction

The capacity for aerial righting in both volant and non-volant taxa enables recovery of body orientation following jumps, accidental falls or mid-air perturbation. The aerial righting reflex and other controlled manoeuvres occur in both wingless insects and vertebrates, and may have predisposed arboreal taxa to the evolution of powered flapping flight [1,2]. Natural selection has presumably favoured the evolution of better righting performance so as to expedite post-righting manoeuvres, including aerial targeting and landing, but specific mechanisms of righting remain unexplored for most taxa. Winged animals can achieve mid-air body rotations through asymmetric flapping motions [3–5], whereas flightless animals use a variety of aerodynamic and inertial means to effect reorientation. Relatively large wingless vertebrates use either body or appendage inertia (e.g. flexion of the torso, rotation of the legs or tail) to effect dorsoventral righting, mostly via multisegmental exchange (and conservation of) angular momentum [6–9]. Aerodynamic and inertial effects may both be present in specific cases. For example, juvenile birds with underdeveloped wings right themselves using active wing movements which may involve both aerodynamic and inertial components [10].

In small flightless arthropods, by contrast, aerodynamic forces on the legs may predominate. For example, small aphids elevate their legs dorsally to effect an aerodynamically unstable profile during upside-down falls, enabling passive body rotation driven by aerodynamic torque [11,12]. In addition to passive aerodynamic righting initiated by reflex actions followed by a constant leg posture, more actively controlled appendicular movements are also feasible. In typical upside-down falls, the righting rotation is coupled with downward acceleration, and thus the relative angle between the incident flow and the insect's coronal plane is constantly changing. As the legs would then be subjected to bilaterally asymmetric aerodynamic loading, compensatory motions may be used to capture and maintain a preferred posture. Although the rapidity of righting can be explained with a simplified model assuming fixed appendage postures, oscillatory flutter induced by rapid rotations (i.e. more than $1000°\,s^{-1}$ [11]) may

significantly delay initiation of post-righting manoeuvres, especially in medium to large sized insects, for which body rotations are presumably not damped by air resistance. Thus, regulation of aerodynamic torques (e.g. gain of body angular momentum) may be functionally advantageous. We hypothesize that asymmetric appendicular motions can help achieve better righting performance for more efficient re-orientational rotations and post-righting manoeuvres. Rapid responses to changing airflow is physiologically feasible for volant insects, given their known capacities to incorporate motion cues via diverse sensory mechanisms, and to respond using in-flight steering with their appendages [13–16]. Similarly, a variety of wingless arthropods use appendicular and axial steering to maintain stability and to manoeuvre during gliding [17–19]. Therefore, we might expect in the aerial righting of flightless insects more active behavioural responses involving feedback and active leg displacement according to aerodynamic context.

To test our hypothesis, we assessed the biomechanics of aerial righting in first-instar nymphs of the stick insect *Extatosoma tiaratum*, MacLeay, 1827, an arboreal species native to coastal eastern Australia. During the rainy season, ground-hatched nymphs walk upwards through vegetational structures to reach the tree canopy. After voluntary drops or accidental falls, nymphal *E. tiaratum* can successfully engage in righting, directed aerial descent and visual targeting to successful landings [20]. We dropped the insects upside-down under controlled conditions and described the three-dimensional kinematics of righting, focusing on leg reflexes and ensuing body motions. The slender geometry of the insects' body and their rigid leg segments permit reconstruction of the spatio-temporal dynamics of righting, including asymmetries of relative air velocities on legs, potentially relevant both to the evolution of controlled aerial behaviours in small invertebrates and to implementation of active stability strategies for aerial robots.

2. Material and methods

2.1. Insect husbandry and morphometrics

Extatosoma tiaratum eggs were incubated under constant air temperature (25°C) and relative humidity (70%). Newly hatched nymphs were collected within the first 24 h and were transferred to clear plastic cups (355–470 ml) with lids. Constant humidity was maintained in the plastic cups by daily water spraying, and all cups were kept in a room at constant temperature (25°C) and 12 L : 12 D cycles. Experimental insects were transported and maintained in the same aforementioned plastic cups between trials. Only healthy, active and intact first instars of age ≤ 1 day were used in experimental trials.

Our biomechanical analyses treated the insect as a system of rigid bodies connected by joints. The insect body was represented as eight sections. The anterior body section (i.e. the head and three thoracic segments) is connected to the abdomen at the median joint (see electronic supplementary materials, figure S1a). The legs were sampled as two sections, namely the femur and the combined tibia and tarsus. The mass of each section was sampled from deep-frozen specimens of equivalently aged instars (N = 10) using an electronic balance (R200D, Satorius AG, Germany). For centre of mass (COM) estimation, each section was first balanced on a horizontally positioned metal pin (diameter 0.3 mm), and the position of the COM was measured based on images taken in top view using IMAGEJ [21]. The dorsally projected planform area, length and width of each segment were measured based on high-definition digital images taken from anaesthetized individuals (N = 10) positioned on a flat surface with legs extended laterally.

2.2. Experimental set-up and protocols

Aerial righting was filmed using two synchronized high-speed video cameras (1280 × 1024 pixels, 500 Hz; HiSpec, FasTec Imaging, CA, USA) as insects fell past a white background illuminated with halogen bulbs. The experimental section was 20–30 cm tall, and the video spatial resolution for the filmed region was more than 2 pixel mm^{-1}. The vertical direction was calibrated using a freely dropped deadweight. Insects were released from a custom-built device which minimized any potential effects of leg–substrate interaction during release. This device consisted of a Teflon-coated plastic angled ridge (with an acute angle of approx. 40°) oriented vertically downward, and a capillary glass tube (diameter approx. 1 mm) positioned in a small hole in the middle of the plastic ridge. Both components were attached to a thick Plexiglas base positioned on a tripod head, the horizontal orientation of which was calibrated with a spirit level. The capillary tube was connected to a vacuum source and a valve system through which air pressure could be controlled (see electronic supplementary materials, figure S2). For each trial, the experimental insect was first placed on a Teflon-coated surface and was then transferred to the release device, with the mesosternum (i.e. the mid-thoracic ventral surface, also close to the COM, being attached via suction to the opening of the capillary tube. A uniform release of the insect was then initiated by rapid equilibration to atmospheric pressure of air within capillary tube. The same device was also used for releasing euthanized controls with fixed leg postures (see electronic supplementary materials, section B).

Video digitization was carried by manually tracking morphological landmarks using commercial software (ProAnalyst, Xcitex Inc., MA, USA). If not visible from either video, landmark positions were estimated using the software's built-in prediction function. The camera system was calibrated in three dimensions using 160 reference landmarks on two reference planes intersecting at 120°. We used a quintic spline function to fit positional data for 19 insect landmarks (electronic supplementary material, figure S1), with the average root mean square error [22] of positional data was about 0.86% in the x-dimension, 0.89% in the y-dimension and 0.18% in the z-dimension. All analyses were conducted using custom-written scripts in MATLAB (R2012a, MathWorks, Natick, MA, USA) and R [23].

2.3. Kinematics of aerial righting performance

A body-fixed frame (H_b) was used to describe body rotation and translation with respect to the spatial frame (H_S; the Z_S axis is vertical and the X_S–Y_S plane is horizontal). The H_b frame was centred at the midpoint of two mid-coxae, and was defined by the X_b axis parallel to the body's longitudinal axis, the orthogonal Z_b axis dorsally oriented and the Y_b axis that is the cross-product of X_b and Z_b (see electronic supplementary materials, figure S1b). Following Murray et al. [24], the translational velocity of H_b was calculated as:

$$v_b = -\dot{R}_b R_b^T p_b + \dot{p}_b = [v_{b,x}, v_{b,y}, v_{b,z}]^T, \qquad (2.1)$$

where R_b and p_b are the rotational matrix and the position of H_b with respect to H_S, respectively. The trajectory of the insect's COM was estimated from the spatial positions of all modelled leg and body sections, with each being simplified as a point mass located at the corresponding position as measured from specimens (electronic supplementary materials, figure S1d). The instantaneous position of the insect's COM with respect to H_S was calculated as:

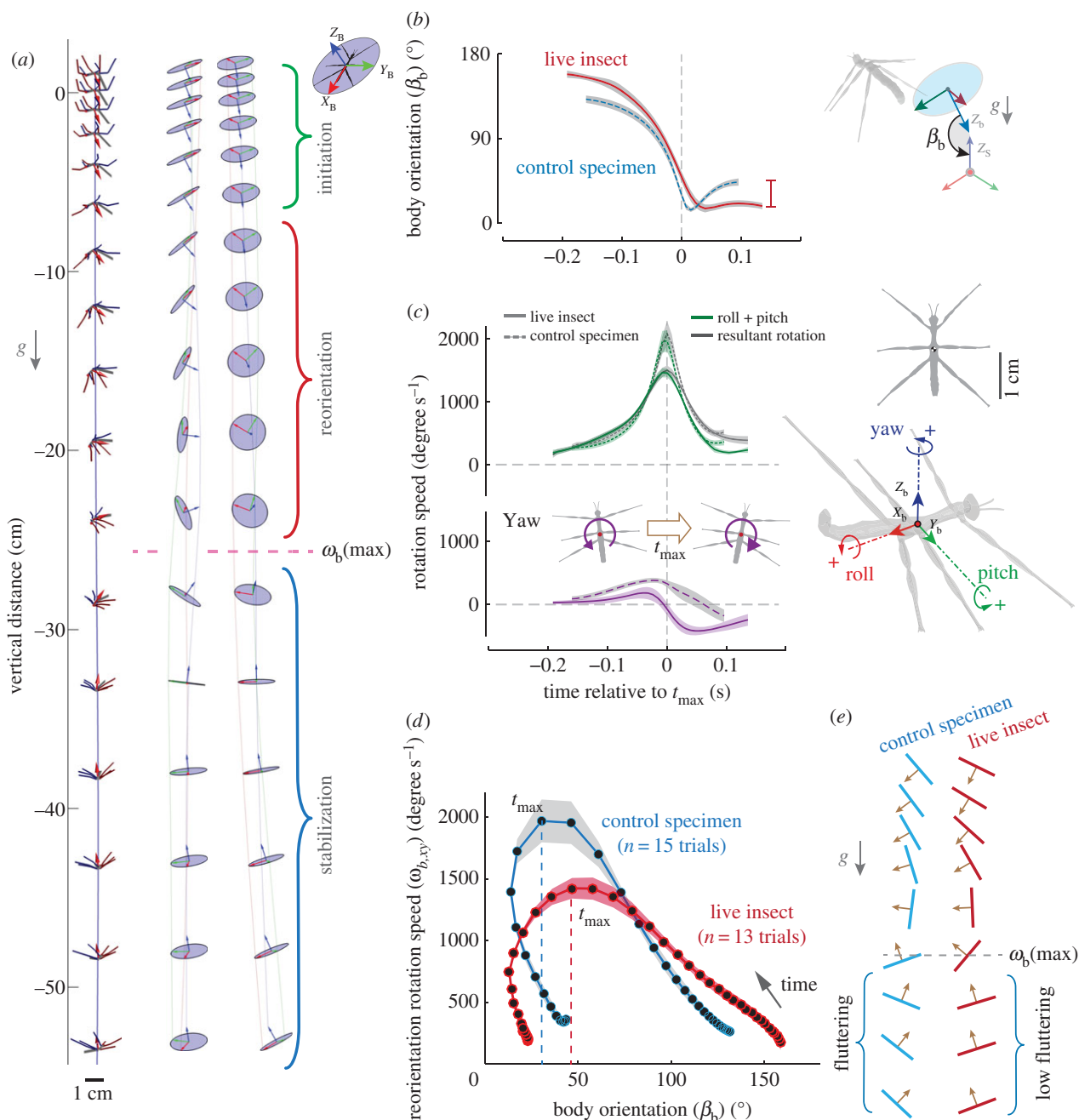$$p_B = m_B^{-1} \sum_{i=1}^{13} m_i p_{m,i}, \qquad (2.2)$$

Figure 1. Aerial righting in nymphal *E. tiaratum*. (*a*) Reconstructed righting trial in lateral view (interval approx. 0.02 s). Body and leg sections are plotted as discrete line segments, with red arrows representing *z*-axis in the body-fixed coordinate frame. Body translations and rotations are also presented in two orthogonal perspectives with the insect represented by a disc fixed at the insect's COM and parallel with the (x_b, y_b) plane. (*b*) Temporal variations in body orientation angle (β_b) with time for live insects and controls (electronic supplementary material, figure S3). (*c*) Comparisons of reorientational angular velocity (top) and angular velocity in yaw (bottom) between live insects and controls. (*d*) Reorientational angular velocity $(\omega_{b,xy})$ as a function of body orientation angle (β_b); interval between points is 8 ms. (*e*) Schematic comparison of reorientation between live insects and controls. Insects are represented by line segments based on mean β_b and arrows represent the dorsal direction (time interval, 24 ms). In (*b*–*d*), shaded curves represent means $\pm$ s.e.m. t_{max}, time when reorientational rotation reached the peak.

where m_B and m_i are the total body mass and section masses, respectively, and $p_{m,i}$ is the spatial position of each segment mass. The position of the COM with respect to H_b was calculated as:

$$p_{B-b} = R_b p_B^T. \tag{2.3}$$

To describe the process of orientation recovery, body orientation angle (β_b; figure 1*b*) was calculated as the angle between the Z_b-axis and the Z_S-axis:

$$\beta_b = \cos^{-1}\left(\frac{z_b \cdot z_s}{|z_b| \cdot |z_s|}\right), \tag{2.4}$$

where z_b and z_S are the axis unit vectors. Then, the insect's rotational velocities were represented by three principal

rotations of H_b:

$$\omega_b = (\dot{R}_b R_b^T)^\vee = [\omega_{b,x}, \omega_{b,y}, \omega_{b,z}]^T, \tag{2.5}$$

also, an 'axis-angle' representation of body rotation was used to describe variation in the orientation of the rotational axis and the relative magnitude of principal rotations:

$$\omega_b = \hat{e}_b \cdot |\omega_b|, \tag{2.6}$$

where $\hat{e}_b = [\hat{\omega}_{b,x}, \hat{\omega}_{b,y}, \hat{\omega}_{b,z}]$ represents the direction of the axis of rotation with respect to H_b, and $|\omega_b|$ is the magnitude of overall rotation (see electronic supplementary material figure S1*b*). For example, $\hat{e}_b = [0,0,1]$ represents positive yaw.
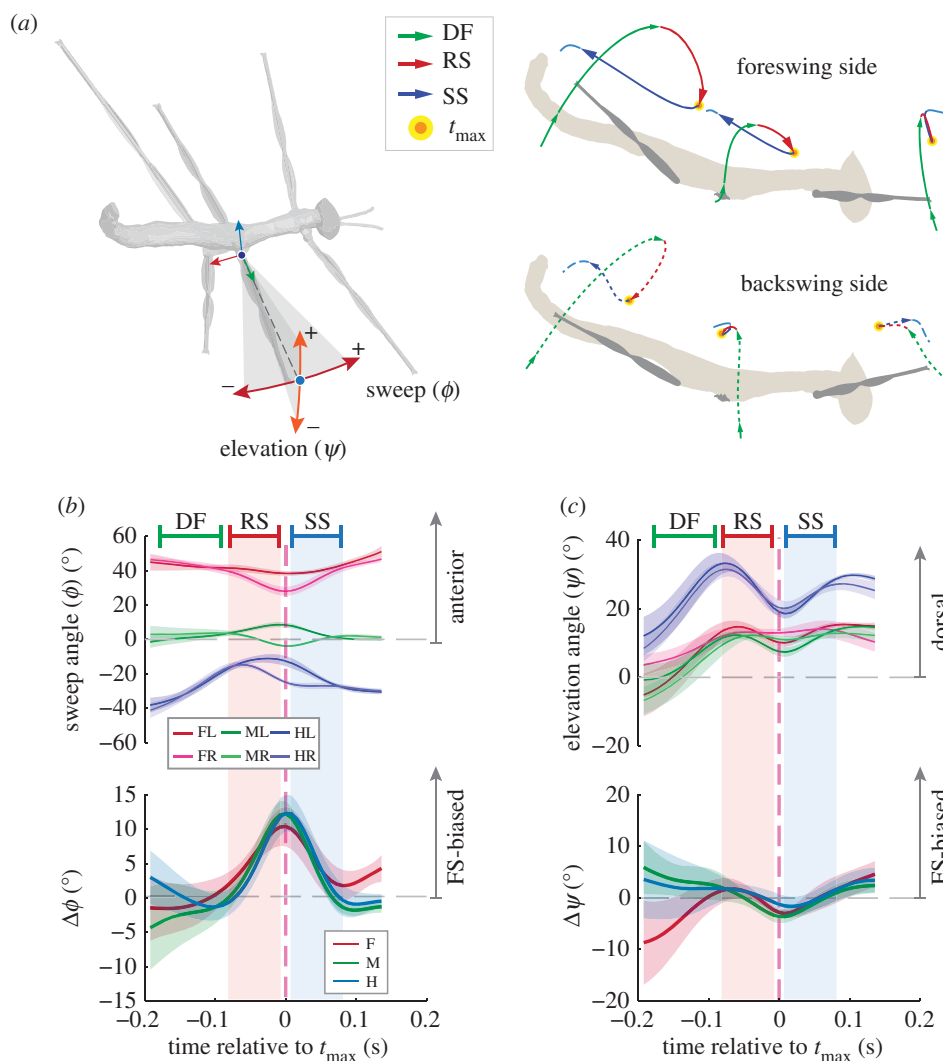
Figure 2. Leg motions in aerial righting. (a) Average leg trajectories with respect to coxa-fixed coordinates in lateral view (DF, dorsiflexion; RS, reorientation strokes; SS, stabilization strokes). (b) Variation of sweep angles and the associated asymmetry index ($\Delta\phi$) through time. (c) Variation of leg elevation angles and the asymmetry index of elevation angle ($\Delta\psi$) through time. F, M and H denote fore-, mid- and hindlegs, respectively; L and R denote left and right, respectively. FS, foreswing side; BS, backswing side. Kinematics data were summarized according to a sinistral-FS standard (see results on leg kinematics).

2.4. Leg kinematics

Swinging movements of each leg were described with respect to a coxa-fixed frame (H_C), the principal axes of which are parallel to those of H_b. Each leg was treated as two sections linked by the tibia−femur joint, each with a coordinate frame fixed at the distal end of the section (see electronic supplementary material, figure S1b). Each section-fixed frame (H_L) is defined by an X_L axis parallel to the longitudinal axis of the section, an Y_L axis parallel to the X_b−Y_b plane and an Z_L axis defined as the cross-product of X_L and Y_L. The angular position of each leg is described by a sweep angle (ϕ) and elevation angle (ψ), the two Euler angles corresponding to rotations of the femur from a lateral position parallel to Y_C (see electronic supplementary material, figure S1c). Given the slender cylindrical geometry of leg sections (e.g. length-to-width ratios range 20−30, see electronic supplementary material, table S1), rotations about the X_L-axes were ignored. To incorporate anatomical directions (i.e. anteroposterior and dorsoventral), positive ϕ represents a forward velocity component (i.e. foreswing), and positive ψ represents a dorsal velocity component (i.e. an upswing). Asymmetry indices of leg postures were calculated as the bilateral differences of posture angles across the sagittal plane (e.g. the asymmetry index of sweep angle $\Delta\phi = \phi_L - \phi_R$, where L and R denote left and right, respectively) (figure 2).

The angular velocities for leg swinging were calculated as the time derivatives of sweep and elevation angles (i.e. $\omega_S = [\dot\phi, \dot\psi]$).

For each leg pair, the asymmetry indices of leg swing velocities were calculated as:

$$\Delta\omega_S = \omega'_{SL} + \omega'_{SR}. \quad (2.7)$$

The signs of ω'_S represent the direction of the swing velocity with respect to the corresponding circular coordinates based on the coxa (the X_C axis for $\dot\psi$ and the Z_C axis for $\dot\phi$). For example, a positive $\Delta\phi$ represents a sinistral swing by both the left and right legs (backswing by the left leg, and foreswing by the right leg; figure 3b). The magnitude of $\Delta\omega_S$ represents the bilateral differences of ω_S; and the sign of $\Delta\omega_S$ represents the directional bias of this difference. For bilaterally symmetric swings, $\Delta\omega_S = 0$.

To assess flow interactions with the legs, each leg was modelled as a cylinder swinging about the coxa. For a given lengthwise position on the leg, the relative velocity induced by leg swinging (U_S) and by body movement (U_B, which is the resultant of translational (U_T) and rotational (U_R) components), together determine the relative air velocity (U) (figure 4a). Relative flow associated with motion of the COM in descent is

$$U_T = R_{B-L}U_{COM}, \quad (2.8)$$

where R_{B-L} is the rotation matrix converting a COM-fixed frame to a section-fixed frame, and U_{COM} is the translational flow
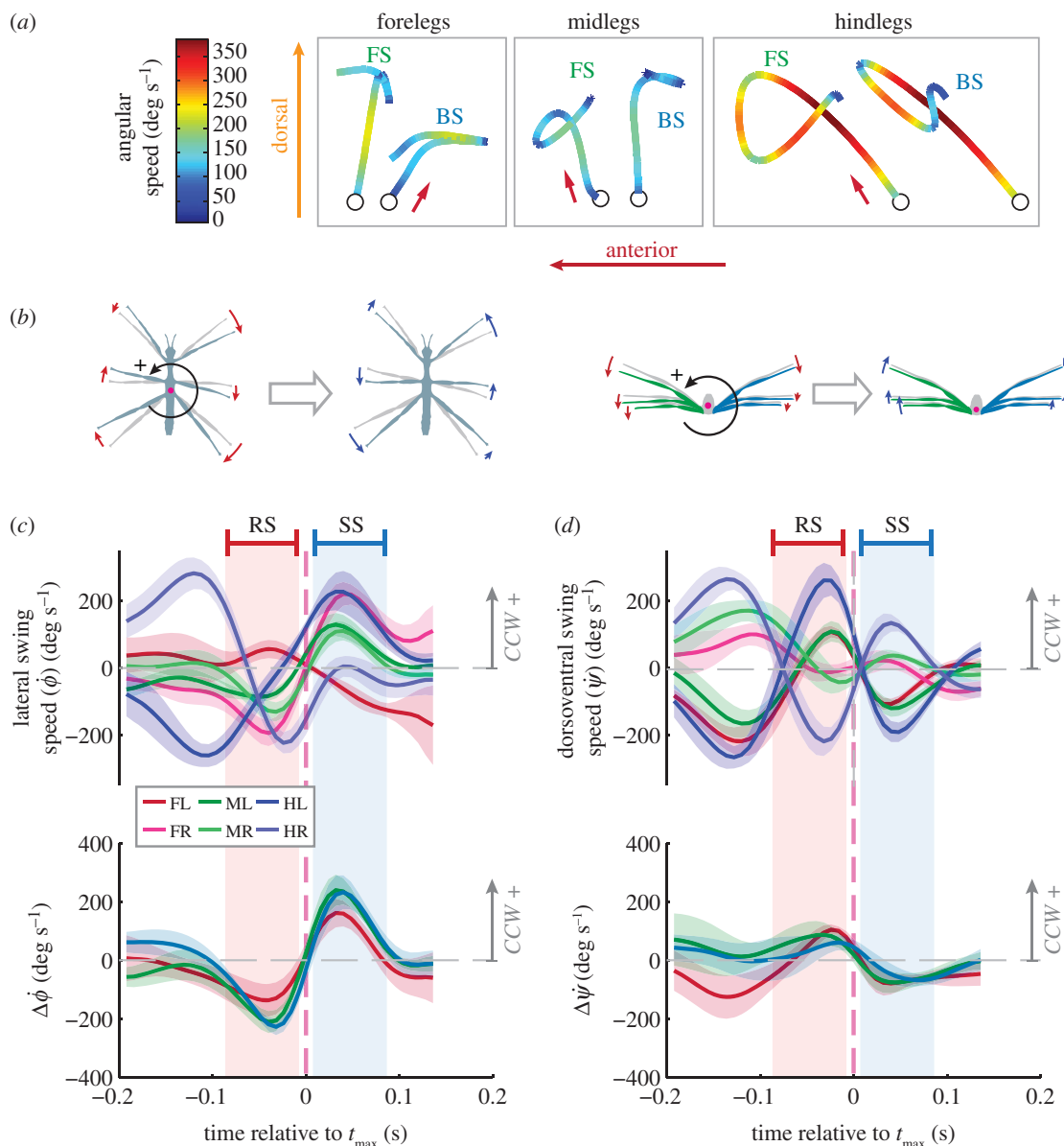
Figure 3. Angular speeds of leg swinging. (*a*) Leg swing trajectories with respect to coxa-fixed frames, colour-coded by angular speed. FS, foreswing side; BS, backswing side. (*b*) Schematic of reorientation and stabilization strokes. Circular arrows denote the positive direction of circular coordinates set at body rotation axes. (*c*) Lateral component of swing velocity ($\dot{\phi}$) and the associated asymmetry index ($\Delta\dot{\phi}$) as functions of time. Counter-clockwise direction (CCW; i.e. sinistral yaw) represents the positive direction of rotation about the Z_b axis. (*d*) Dorsoventral component of swing velocities ($\dot{\psi}$) and the associated asymmetry index ($\Delta\dot{\psi}$) as functions of time. The counter-clockwise direction (CCW; i.e. sinistral roll) represents the positive direction of rotation about the X_b axis.

velocity. Relative flow associated with body rotation is given by:

$$U_R = \omega'_B r_B, \qquad (2.9)$$

where r_B is the distance from a given point on a leg section to the COM. Relative flow induced by leg swinging is given by:

$$U_S = \omega_S r, \qquad (2.10)$$

where r is the distance from the coxa to a given point along the leg. With respect to the section-fixed frames, U was represented by three components: (i) the longitudinal component (U_x); (ii) the lateral component (U_y), which is parallel to the X_C-Y_C plane and is influenced by lateral component of fore- and backswings of the leg; figure 4*a,b*; and (iii) the dorsoventral component (U_z), which is coplanar with the Z_b axis and affected by dorsoventral components of leg swinging (i.e. the up- and downswings). Reynolds number for each leg was calculated as: $Re = \rho L \bar{U}/\mu$, where ρ is air density, L is characteristic length (either leg length or mean diameter), $\bar{U}$ is relative velocity sampled at the midpoint of a leg and μ is air kinematic viscosity.

To summarize bilateral differences between legs and to assess how they relate to yaw and reorientation, we introduced asymmetry indices for each velocity component. The asymmetry index of a given component represents: (i) the magnitude of bilateral differences across the rotational axis and (ii) the directional bias with respect to the insect's body rotation. To analyse the correlation between relative velocities and body rotation, the insect was simplified as a point mass with mobile appendages (i.e. ignoring the distance between the coxa and the COM; figure 4*b*). Torque production is thus directly affected by the normal components of relative air velocities on legs (e.g. U_y and U_z), which can be represented with respect to circular coordinates associated with corresponding rotations. Specifically, body yaw and lateral components of relative velocities share the Z_b axis as the polar axis; similarly, reorientations and dorsoventral components of relative velocities share the axis of the resultant of roll and pitch (i.e. $\hat{e}_{b,xy}$) as the polar axis. For relative air velocities sampled on each tarsus, the asymmetry index is:

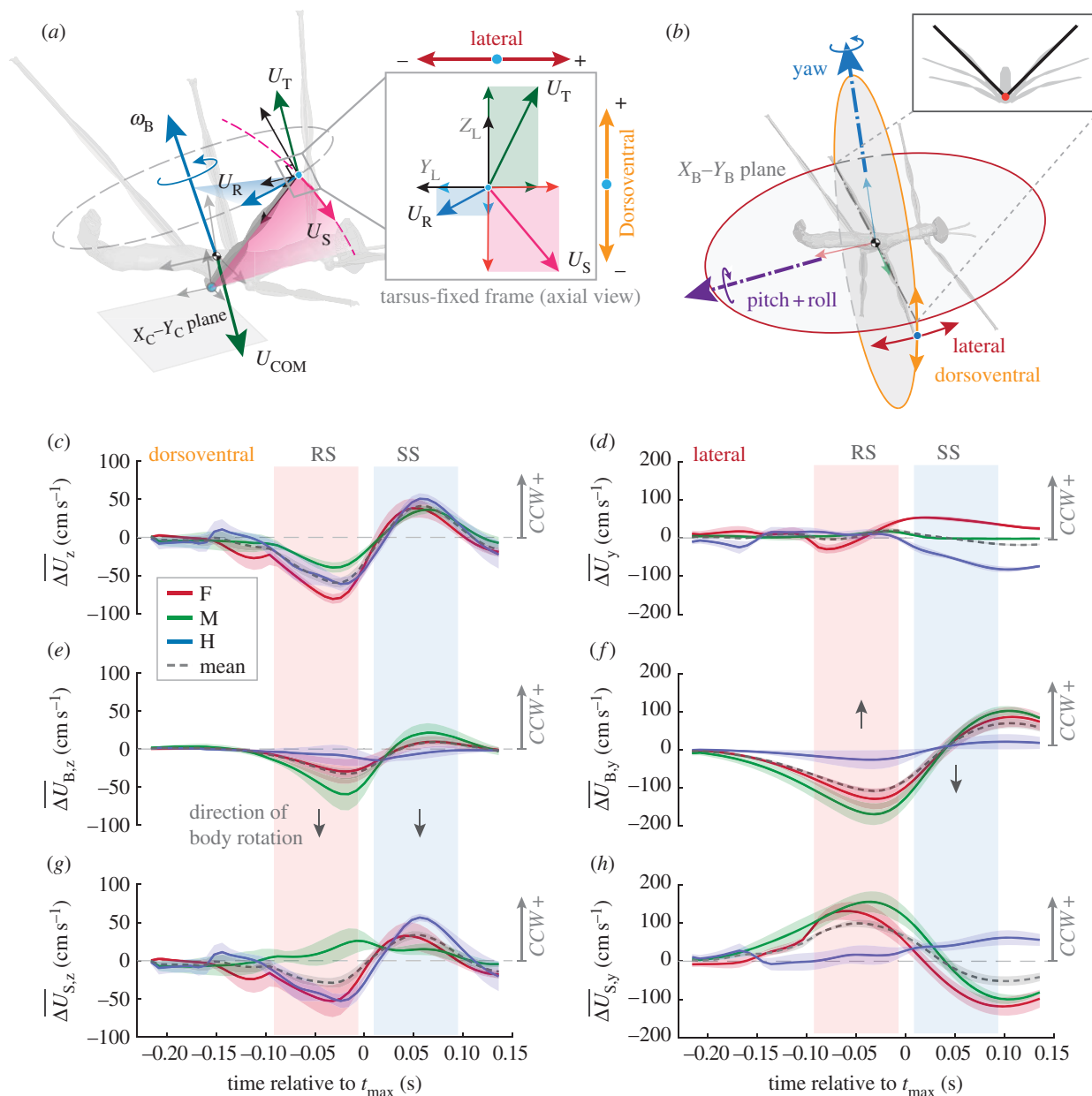$$\Delta U = U'_L + U'_R, \qquad (2.11)$$

Figure 4. Leg and body translations in aerial righting. (*a*) Relative air velocity (*U*) at a given longitudinal position on the leg consists of three components: the body rotation-induced velocity (U_R), the body translation-induced velocity (U_T) and the leg swing-induced component (U_S). (*b*) Geometry of the simplified model used for representation of reorientational rotations. (*c,d*) Mean asymmetries through time in velocity (*U*) components for each leg pair. (*e,f*) Mean asymmetries through time in U_B for each leg pair. (*g,h*) Mean asymmetries through time in U_S for each leg pair. Velocity values represent averages for the two leg sections; dashed lines represent means of three leg pairs. Shaded curves are means $\pm$ s.e.m. Plots follow the same directional configuration as in figure 4*b*.

where the sign of U' is expressed with respect to the corresponding circular coordinates. ΔU is the resultant of ΔU_B and ΔU_S, and ΔU_S represents bilateral differences in leg swing-induced relative velocities. For example, when ΔU_S has the same sign as ΔU_B, legs move similarly in the flow field. The asymmetry indices of dorsoventral components (U_z) were corrected by multiplying $\sin(\theta_{x,y})$, where $\theta_{x,y}$ is the intersection angle between $\hat{e}_{b,xy}$ and the Z_b axis (see electronic supplementary material, figure S8*e*).

2.5. Aerodynamic effects

Aerodynamic effects were addressed based on the angular dynamics of insect sections as a system of rigid bodies, and we thus ignored any potential damping between joints and along with elastic energy storage in muscles. Aerodynamic interactions between a falling insect and the ambient flow apply an aerodynamic torque (τ_A) about COM and cause changes to the total angular momentum (M_B), whereas angular acceleration of

leg swings induces inertial torque (τ_I) and can alter orientation of the body-fixed frame (H_b). The observed angular acceleration of H_b is $\dot{\omega}_b = \tau_A/I_B + \tau_I/I_b$, where I_B and I_b are total mass moment of inertia about the COM and moment of inertia of body sections, respectively.

A COM-fixed frame (H_B) was used for all calculations of angular momentum, with all axes parallel to those of H_b. M_B consists of rotations of all insect sections with respect to H_S, and movements of all mobile sections (i.e. of the abdomen and legs) with respect to the COM; M_B was calculated as $M_B = M_b + M_I$. M_b is the angular momentum of body sections and was calculated as:

$$M_b = r_a \times m_a v_a + r_j \times m_p v_j + r_{pj} m_p v_{pj}, \tag{2.12}$$

where *m* is mass, *v* is velocity, *r* is the vector from the COM to a point mass, '*a*' denotes the anterior body sections, '*p*' denotes the posterior body section, *j* denotes median joint, *pj* denotes the velocity of the posterior section with respect to the median joint, v_a and v_b are

velocities of two body sections with respect to the COM and v_{Pj} is the velocity of the posterior section with respect to median joint. M_l is the angular momentum of the legs and was calculated as:

$$M_l = \sum_{j=1}^{6} r_j \times m_j v_j + \sum_{i=1}^{12} r_i \times m_i v_i, \qquad (2.13)$$

where j denotes each of six legs, m_j is the mass of each leg, r_j is the vector from the COM to a given coxa, v_j is the velocity of a coxa with respect to the COM, i denotes 12 leg sections, m_i is the mass of each section, r_i is the vector from the corresponding coxa to m_i and $v_i = \omega_i \times r_i$ is the translational velocity of m_i with respect to the coxa-fixed frame (H_C). For each principal rotation, the aerodynamic torque acting on the COM was calculated as: $\tau_A = dM_B/dt$.

3. Results

3.1. Rotational behaviour in aerial righting

After being released upside-down, nymphs righted themselves with a rapid dorsoventral rotation during descent (see electronic supplementary materials, movie S1). The COM of the insect accelerated downwards nearly vertically (e.g. a horizontal deviation from initial position <2 cm for a typical drop of 31 cm). Recovery of the right-side-up orientation was completed (i.e. the body orientation angle reached a minimum value; figure 1b) at 0.30 ± 0.07 s (mean $\pm$ s.e.m.) after release, with a COM height loss of 30.9 ± 6.4 cm (i.e. approx. 18 body lengths; $N = 4$ individuals, with three to four drops per individual). Also, since roll and pitch are coupled during this dorsoventral rotation (see below), we treated righting as a combination of two rotational processes: yaw rotation and reorientational rotation (i.e. the resultant of roll and pitch). Based on the phases of body rotations and leg behaviours (see below), we segregated timing of righting performance into three stages: (i) an initiation phase characterized by brief body rotation and dorsiflexion of legs; (ii) a reorientation phase during which the insects performed rapid dorsoventral flipping and reached the maximum reorientational rotation speed; and (iii) a stabilization phase during which the insects underwent angular deceleration (figure 1a,c).

During the initiation phase, reorientational rotation of body proceeded from $0° s^{-1}$ to $478 \pm 42° s^{-1}$ (i.e. approx. 33% of the maximum; $\beta_b = 141.9 \pm 5.6°$, approx. 14% of total orientation recovery) as the legs extended and moved dorsally, with the insect COM descending to 6.5 ± 1.5 cm from the drop point (figure 1a). Second, reorientational rotation accelerated and reached the peak at time t_{max} (e.g. a maximum rotational velocity of $1560 \pm 220° s^{-1}$, and the COM averaging a vertical speed of -170.4 ± 7.8 cm s^{-1}). The insects performed the major portion of reorientational rotation by t_{max} (i.e. $\beta_b = 49.4 \pm 5.6°$, corresponding to approx. 71% of total orientational recovery). Since t_{max} is the most recognizable time point for body rotation dynamics and is the temporal midpoint between two major leg reflex phases (see below), we treated it as a temporal reference point for summarizing body and leg kinematics. Finally, during the stabilization phase, the insects suddenly decelerated in reorientational rotation and maintained a stable dorsoventral posture with only minor oscillation (e.g. oscillation amplitudes averaging $13.4 \pm 4.0°$; figure 1a,b).

Whereas all three principal rotations contributed to righting, the peak rotation (i.e. when $\omega_B \geq 90\% \omega_{B,max}$) was primarily derived from rotations in roll and pitch, with relatively limited contributions of yaw (e.g. the fraction of yaw to total rotation averaged only $15 \pm 5\%$; electronic supplementary material, figure S3 g). Notably, at t_{max} rapid directional reversal of yaw occurring once a peak value was attained (figures 1c, figure 5b). During the stabilization phase, yaw predominated over roll and pitch, with approximately 70% of the insects' rotational energy being associated with yaw (figure 5c).

Despite similar reorientations between falling live insects and control specimens (euthanized individuals with fixed leg postures; $N = 3$ individuals, with four to six drops per individual; see electronic supplementary materials section B, movie S2), active leg movements contributed substantially to body rotation dynamics. First, control specimens showed significantly greater rotational velocities during reorientation, and exhibited more fluttering relative to live insects; they also showed no directional reversal of yaw (figure 1c). Live insects showed an earlier acceleration of body rotation (e.g. when $\beta_b = 100°$, and $\omega_{b,xy}$ reached approx. $1000° s^{-1}$ in live insects compared with only approx. $750° s^{-1}$ in control specimens; figure 1d), reached peak rotation at an earlier stage (e.g. at t_{max}, with β_b averaging $49.4 \pm 5.5°$ and $30.4 \pm 3.3°$ in live insects and control specimens, respectively), and completed aerial righting with less fluttering (e.g. maxima of β_b being $16.8 \pm 4.1°$ and $42.1 \pm 6.1°$ in live insects and control specimens, respectively). Furthermore, live insects completed both reorientation and stabilization phases with significantly lower aerodynamic work compared to control specimens (figure 5d). Together, these results suggest that active leg movements reduced the net gain of rotational energy during the initiation and reorientation phases.

3.2. Kinematics of aerial righting reflexes

Immediately after losing tarsal contact, the insects attempted to retrieve contact by ventrally extending their legs (i.e. via plantar flexion around the coxa–trochanter and tibia–femur joints; see electronic supplementary materials, movie S3). After unsuccessful contract retrieval from the release surface, legs performed three sets of actions corresponding with the three righting phases described above. During the initiation phase, the insects performed bilaterally symmetric dorsiflexion (DF, at 0.12 ± 0.03 s after release), extending and elevating all legs dorsalward (initiation time of femur elevation averaged 5 ± 3 ms, 7 ± 6 s and 2 ± 2 ms for the fore-, mid- and hindlegs, respectively). This dorsiflexion was completed within 0.3 ± 0.03 s, and induced a minor dorsalward displacement of the COM (e.g. by 2.1 ± 0.1 mm; see electronic supplementary material, figure S4). This postural transformation presumably shifted the centre of pressure dorsally away from the COM, thus promoting passive rotation driven by aerodynamic torque on the legs while falling upside-down [11].

During the reorientation and stabilization phases, leg trajectories were bilaterally asymmetric. Two stroke actions, termed the reorientation stroke (RS) and the stabilization stroke (SS), were designated based on smooth intervals of motion based on axis-angle representations (figure 2a; see electronic supplementary material, figure S5). Asymmetries in average speed, amplitude and orientation of the RS and SS were specific to each leg pair (see electronic supplementary material, figure S6). These bilateral asymmetries in leg kinematics and their correlation with body movements were
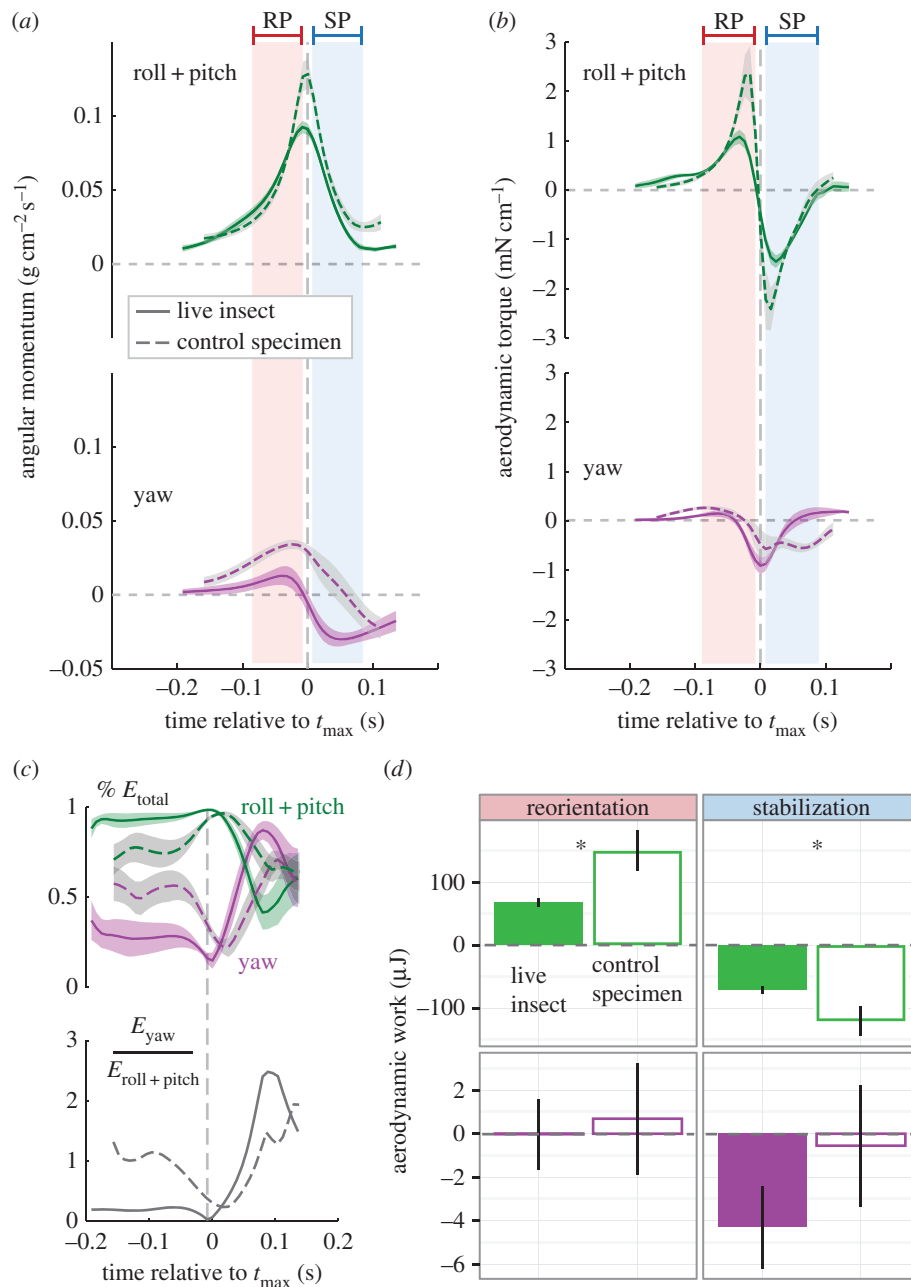
Figure 5. Dynamics of mid-air reorientation. (*a*) Temporal dynamics of angular momentum through time, and (*b*) aerodynamic torque associated with reorientational rotation and yaw. (*c*) Temporal variation in relative rotational energies associated with the reorientational rotation and yaw. In (*a*–*c*), shaded curves represent means ± s.e.m. (*d*) Comparison of total aerodynamic work through time between live insects and control specimens. Values are means ± s.e.m. Asterisks denote significant differences between means. RP, reorientation phase; SP, stabilization phase.

more clearly shown by the dynamics of sweep (ϕ) and elevation (ψ) angles, which are the Euler angles representing leg postures in lateral and dorsoventral orientations, respectively. In the lateral orientation, aerial righting reflexes appeared as bilaterally asymmetric fore- and backswings, with the ipsilateral legs swung in the same direction and overlapping with peaks of sweep angle asymmetry ($\Delta\phi$) near t_{max} (figure 2*b*). In the dorsoventral orientation, legs first performed downswings and then transitioned to upswings at t_{max}, at which time the peaks of elevational angle asymmetry ($\Delta\psi$) were reached (figure 2*c*). Remarkably, although both swing velocity components ($[\dot{\phi}, \dot{\psi}]$) exhibited leg pair-specific dynamics, their asymmetry indices ($[\Delta\dot{\phi}, \Delta\dot{\psi}]$) were temporally coordinated among the three leg pairs (electronic supplementary material, figure S7).

Based on the direction of the lateral component of swing velocity during reorientation phases ($\dot{\phi}$; i.e. the fore- and backswing), we designated one leg side as the 'foreswing side' (FS;

figure 2), and the contralateral leg side as 'backswing side' (BS). The chirality of FS was correlated with the direction of body yaw prior to reorientation phase. In six of 13 trials, insects exhibited a sinistral FS while performing sinistral yaw during initiation phase (i.e. positive rotation about the Z_b axis; counter-clockwise in dorsal view). In other trials, a dextral FS was coupled with dextral yaw (i.e. negative about the Z_b axis). For clarity, we hereafter summarize body and leg kinematics based on a sinistral-FS standard by mirroring the data from trials with dextral-FS about the sagittal plane. Following this sinistral-FS configuration, the two rotational processes of righting showed clear transitional patterns during reorientation and stabilization phases: (i) body yaw transitions from sinistral to dextral direction (figure 1*c*) and (ii) reorientational rotations consisting of dextral roll (clockwise about X_b axis) and pitch in various directions, as represented by an anteriorly oriented rotational axis (electronic supplementary material, figure S3*g*).
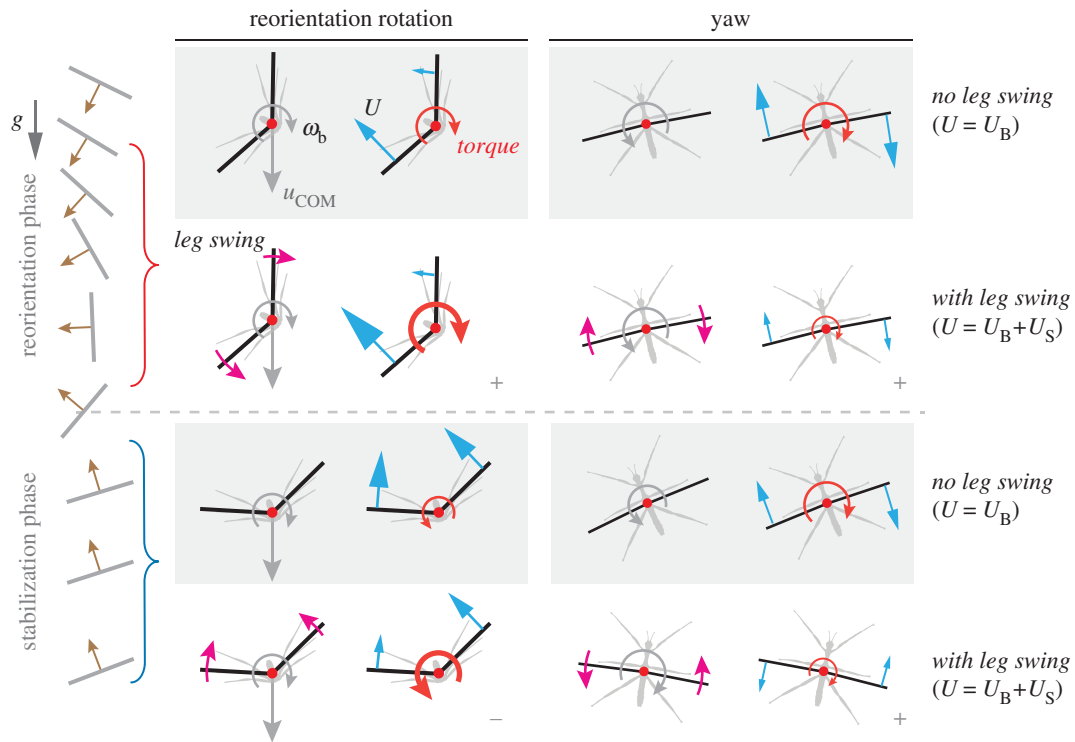
Figure 6. Schematic of torque regulation in aerial righting. The size of blue arrows represents the magnitude of the normal component of relative air velocity on legs. Reorientational rotations are represented by roll for simplicity. '$+$' and '$-$' represent positive and negative contributions of leg swings to body rotation, respectively. The dorsoventral components of swings first promote rotation and then impede it. The lateral components of swings enhance body yaw by reducing total torque.

3.3. Functionality of aerial righting reflexes

Temporal dynamics of the body movement-induced flow field (U_B) on each leg was not only associated with body rotation and translation, but also on leg postures which changed throughout righting (see electronic supplementary materials, section F). The magnitude of the translational component on the legs (U_T) predominated over that of the rotational components (U_R). For example, U_R at t_{max}, was approximately $0.26\ \mathrm{m\ s^{-1}}$ on the tarsus (based on a 1 cm leg length), the magnitude of which is only approximately 17% of that of U_T (i.e. approx. $1.5\ \mathrm{m\ s^{-1}}$). Whereas both U_T and U_R exhibit significant bilateral asymmetries on the legs, the magnitude of the former was about one order of magnitude greater than that of the latter (see electronic supplementary material, figure S10 and table S2). In the ideal cases with no leg swinging (e.g. as characterizes control specimens), U_B is the only source of relative flow, and its role to the insect's rotation can be represented by the relative directions between the asymmetry of U_B (ΔU_B) and body rotation ω_B (e.g. co-directional ΔU_B and ω_B indicate torque generation that promotes body rotation; figure 6).

During dorsoventral righting, contralateral legs across the rotational axis (e.g. outside versus inside legs) experience temporal lags intersecting the translational flow (e.g. inside legs would intersect flow at a higher angle of attack prior to the outside legs), thereby creating a bilaterally asymmetric loading ($\Delta U_{B,z}$; figure 4e). This asymmetry is enhanced by downswings of reorientational strokes by approximately 100% (ΔU_z; figure 4), increasing aerodynamic torque and promoting body rotation. Also, a reverse process occurs after t_{max} when upswings of the stabilization strokes reverse directional bias of the relative flow asymmetry (i.e. reversed ΔU_z and an approx. 100% increase of $\Delta U_{B,z}$;

figure 4), thus enhancing counter-torque production that resists body rotation.

By contrast, the lateral components of the relative air velocity (U_y) on the legs was highly influenced by fore- and backswings throughout righting. Fore- and backswings generally offset the bilateral asymmetry in $U_{B,y}$, which reduced values ΔU_y and resulted in a major reduction of flow resistance to body yaw (figure 4).

Thus, relative air velocity was influenced by leg swinging, speeding up the dorsoventral flip and regulating yaw. This conclusion is supported by a correlation between asymmetry in the relative air velocity (ΔU) and the magnitude of aerodynamic torque (electronic supplementary material, figure S11). We present a simplified model to summarize mechanisms used for reorientation and stabilization in aerial righting (figure 6). The analyses based on a rigid body model also indicated that aerodynamic torques predominate over inertial torques throughout righting. For each principal rotation, inertial torque induced by leg swings was one order of magnitude smaller than the estimated aerodynamic torque (electronic supplementary material, figure S13). Based on observed leg kinematics, an inertia-only model predicted a cumulative yaw of less than 1% of observed values, and a cumulative reorientation of less than 25% of the observed value, both of which are clearly insufficient for completing the observed body rotations.

4. Discussion

4.1. Kinematics and control of aerial righting

Nymphal righting in *E. tiaratum* is rapid and smooth, and derives from aerodynamic torques regulated through

bilaterally asymmetric leg swinging as it interacts with airflow during descent. These leg swings are characterized by smooth stroke intervals and sharp reversals, the pattern of which differs from those kinematics expected in inertially dominated righting (e.g. circular movements of inertial appendages [25]). Leg strokes are presumably effective in achieving high translational speeds and in generating sustained aerodynamic moments, as the magnitude of associated aerodynamic force scales with the square of relative velocity. Sustained stroking movements may also be more efficient in overcoming damping effects between joints.

Stroke kinematics are presumably constrained by anatomical features and movement capabilities of the legs. For example, stroke amplitude is likely limited by flexibility in the coxa–trochanter joints, and the angular speed will be constrained by the torque production at the joint. Furthermore, leg inertia and body size may influence the temporal pattern of strokes. Compared with wings, legs bear greater inertia and a lower aerodynamic loading. Yet the temporal frequency of leg strokes here (e.g. frequency 12–20 Hz) falls within the range of wingbeat frequencies for small insects (e.g. wingbeat frequency ranges from 6 to 316 Hz for insects of body mass approx. 25 mg [26]). Righting and leg swinging at low amplitude but high frequency may characterize aerial righting in a variety of flightless arthropods of similar sizes.

The series of righting reflexes documented here, with both bilaterally asymmetric and symmetric movements, represents a sequence of control outputs more complex than previously indicated in other taxa (e.g. a single reflex action of leg dorsiflexion in aphids [11]). Bilaterally symmetric dorsiflexion is the immediate reaction after unsuccessful contact retrieval. Elevating appendages dorsally is probably a basic reflex response to the loss of foothold, given its occurrence in numerous wingless and winged arthropods in both terrestrial and aerial contexts [13–15,27,28]. Also, movements are coordinated here among ipsilateral legs. Given coordination involving three leg pairs, bilateral asymmetries in stroke amplitude and orientation are likely generated through centralized rhythmic control, and temporally coordinated asymmetries of swing speed between leg pairs may maximize aerodynamic torques (see below). Furthermore, such kinematic organization of the legs, distinct from those in walking (e.g. double-tripod gait), exhibits convergence with wing stroke movements in insects using two aerodynamically functional wings [26], and with some swimming crustaceans using multiple pairs of appendages (e.g. remipedes [29]).

Among all sensory cues, body orientation with respect to gravity may serve as the most basic reference and be integrated with other signals. Also, various sensory inputs are involved in different stages of righting. For example, feedback of tarsal contact and the direction of incident airflow can be important cues for initiation of righting. Visual cues are presumably critical for control of leg behaviours during the reorientation and stabilization phases. Bilateral differences in aerodynamic loading on the legs and wind-sensing hairs [30] may also assist in sensing the state of body rotation. Further studies may introduce a variety of initial conditions (e.g. dorsoventral orientation, and rotational and translational velocities) and experimentally modified morphological asymmetries (e.g. leg length) to examine the robustness of the righting reflexes, as well as to understand the control mechanisms of leg reflexes.

4.2. Functional significance of aerial righting reflexes

Comparison of righting dynamics between live insects and control specimens shows reduction in height loss and earlier initiation of post-righting performance, which may be advantageous in natural conditions. Leg reflexes interact with the airflow derived from body translation to influence temporal patterns of torque generation, to promote reorientation and to reduce fluttering. Together, these enable righting efficiency in both spatial and temporal scales greater than those driven by passive aerodynamic mechanisms based on stereotypic leg postures [11]. From an energetic perspective, mid-air righting is essentially a sequence of gaining and dissipating rotational energy, and the aerial righting reflexes described here limit net gain of rotational energy during the reorientation phase, and subsequently facilitated its dissipation.

Aerial righting behaviours are distinct from those used in-flight manoeuvres by volant taxa (e.g. bilaterally asymmetric postural control in locusts and fruit flies [16,31]). Coupling between linear descent and self-rotation generates a net flow field which rapidly reorients between dorsal and ventral directions of the insect, and thus the dorsoventral component of leg swings can effectively interact with flow and be used to regulate torques. Aerodynamic effects were shown here to predominate, although insect legs may exhibit greater inertial effects under other initial conditions (e.g. immediately after jumping [32]). The reorientational rotation of *E. tiaratum* nymphs features combinations of roll and pitch in variable relative proportions, but does demonstrate consistent dynamics in yaw. Yaw motions were coupled with dorsoventral reorientation, although they do not directly contribute to the dorsoventral flip. The lack of association between roll and pitch may be attributed to comparable effectiveness of aerodynamic torques about the longitudinal and lateral axes, in turn deriving from the specific body plan of these stick insects (e.g. the distributions of projected planform area and of mass are nearly symmetric anteroposteriorly about the COM; see electronic supplementary material, figure S1).

Manoeuvring responses for correcting dorsoventral orientation and heading are presumably common in wingless arthropods performing controlled aerial descent within naturally turbulent regimes, and we expect a wide variety of appendicular behaviours specific to the particular body-flow configuration and desired manoeuvres. For example, wingless *Cephalotes* ant workers rapidly swing their legs for control during directed aerial descent, with angular limb speeds exceeding $150° \text{ s}^{-1}$ [12]). Comparable studies of aerial manoeuvring among arthropod species of different morphologies (e.g. body plan and relative leg size; also, figure 7) would enhance understanding of different leg kinematics and associated inertial and aerodynamic contributions to righting performance. Sampling through an ontogenetic sequence for the same species would similarly address allometric scaling of these effects.

4.3. Aerial righting reflexes and the origins of controlled aerial manoeuvres

Bilaterally asymmetric movements of different body structures (e.g. legs, antennae and cerci in flightless arthropods, and winglets or partial wings in protopterygotes) may be key features in the evolution of controlled aerial behaviours. Our results support the hypothesis that selection for better aerial
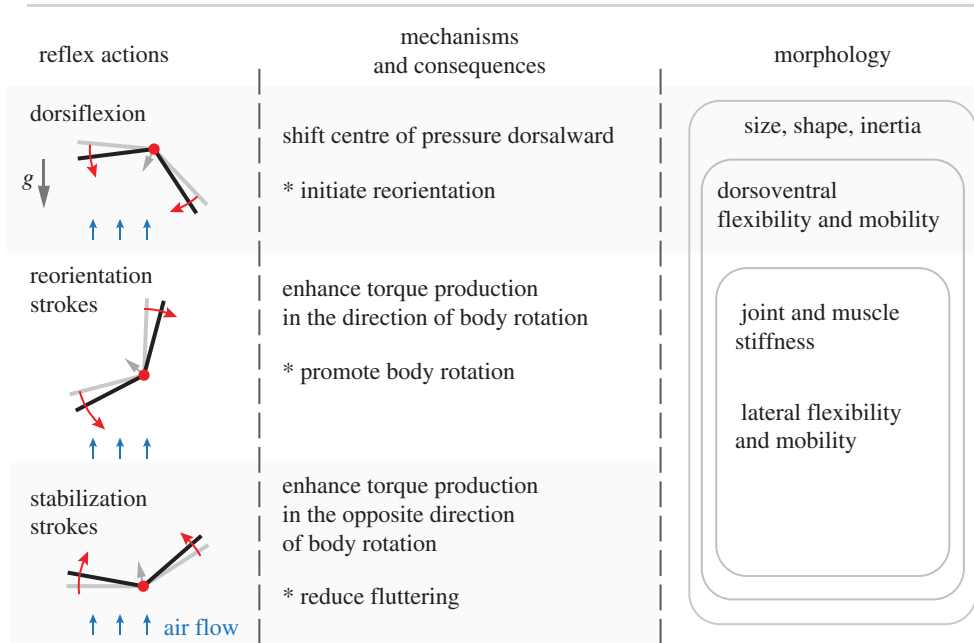
appendicular features

reflex actions	mechanisms and consequences	morphology

Figure 7. Summary of relevant appendicular features for aerial righting reflexes. In the left column, insects are represented by a point mass with one pair of appendages; arrows denote the dorsal direction. For morphological features, a Venn diagram shows inclusion of more features as righting proceeds.

righting and associated leg motions may underpin origins of other types of manoeuvring or the incipient flapping of early wings [2,26]. Righting performance of arthropods will be influenced by a number of interrelated factors, including body plan, aerodynamic and inertial properties of appendages, and joint flexibility (figure 7). Also, translational and rotational movements prior to righting, along with the body-flow field interaction (e.g. the incident flow angle with respect to the dorsoventral orientation) will influence how body rotation proceeds. In addition to aerodynamically relevant morphological variables, inertial properties of appendages can also influence whole-body kinematics. Appendage posture can significantly alter the whole insect's moments of inertia about principal axes, as well as the relative positions of the COM and of aerodynamic pressure. For example, insects with legs shorter than those nymphal *E. tiaratum* (e.g. lepsimatid apterygotes [33]) may reorient primarily using body roll rather than pitch, given a much lower moment of inertia about the longitudinal body axis. Feedback mechanisms that enable leg kinematics to respond to a constantly changing flow field would be favoured by selection. At the lower level of control, the ability to coordinate ipsilateral appendages and to generate bilaterally asymmetric kinematics would also enhance the efficacy of aerial manoeuvres.

Various features of protowings, including their size and shape, mobility in both dorsoventral and anteroposterior directions, control of bilaterally asymmetric movements and coordination among ipsilateral winglets, would all be biomechanically relevant to the ability to right aerially, along with other features of controlled falling and gliding behaviour. Active appendicular motions interacting with and using the surrounding flow field would facilitate righting and subsequent postural control for any jumping or falling arthropod. Similarly, in the origins of vertebrate flight, righting and control prior to the origins of wings may have influenced the evolution of aerodynamically functional wings, although inertial effects likely played more significant roles relative to the much smaller flying arthropods [1,10,34,35]. The kinematics and control features of aerial righting in small arthropods, as summarized in figure 7, are also potentially applicable to any small robotic device with projecting appendages (e.g. wings and legs) that can be used to generate aerodynamic torques. Orientational and rotational information from flow sensors, gyrosensors and gravisensors could be incorporated into control of appendicular kinematics. For winged robots, bilaterally asymmetric motions can be engaged to enhance torque and countertorque production for rapid righting following upside-down falls, mid-air perturbation or extreme manoeuvres. Introduction of the capacity for aerial righting capability would improve robustness in insect-sized flying robots (e.g. 'RoboBee' [36]). Moreover, multi-legged land robots (e.g. an insect-sized hexapedal robot [37]) could use aerial righting for mid-air recovery after falling from heights. For either winged or legged robots, a mix of aerodynamic and inertial effects may be used to optimize recovery strategies in a variety of adverse circumstances.

References

1. Jusufi A, Zeng Y, Full RJ, Dudley R. 2011 Aerial righting reflexes in flightless animals. *Integr. Comp. Biol.* **51**, 937–943. (doi:10.1093/icb/icr114)

2. Dudley R, Yanoviak SP. 2011 Animal aloft: the origins of aerial behavior and flight. *Integr. Comp. Biol.* **51**, 926–936. (doi:10.1093/icb/icr002)

3. Warrick DR. 1998 The turning- and linear-maneuvering performance of birds: the cost of efficiency for coursing insectivores. *Can. J. Zool.* **76**, 1063–1079. (doi:10.1139/z98-044)

4. Iriarte-Díaz J, Swartz SM. 2008 Kinematics of slow turn maneuvering in the fruit bat *Cynopterus brachyotis*. *J. Exp. Biol.* **211**, 3478–3489. (doi:10.1242/jeb.017590)

5. Ristroph L, Bergou AJ, Ristroph G, Coumes K, Berman GJ, Guckenheimer J, Wang ZJ, Cohen I. 2010 Discovering the flight autostabilizer of fruit flies by inducing aerial stumbles. *Proc. Natl Acad. Sci. USA* **107**, 4820–4824. (doi:10.1073/pnas.1000615107)

6. Kane T, Scher MP. 1969 A dynamical explanation of the falling cat phenomenon. *Int. J. Solids Struct.* **5**, 663–670. (doi:10.1016/0020-7683(69)90086-9)

7. Edwards MH. 1986 Zero angular momentum turns. *Am. J. Phys.* **54**, 846. (doi:10.1119/1.14429)

8. Fish FE, Nicastro AJ, Weihs D. 2006 Dynamics of the aerial maneuvers of spinner dolphins. *J. Exp. Biol.* **209**, 590–598. (doi:10.1242/jeb.02034)

9. Jusufi A, Goldman DI, Revzen S. 2008 Active tails enhance arboreal acrobatics in geckos. *Proc. Natl Acad. Sci. USA* **105**, 4215. (doi:10.1073/pnas.0711944105)

10. Evangelista D, Cam S, Huynh T, Krivitskiy I, Dudley R. 2014 Ontogeny of aerial righting and wing flapping in juvenile birds. *Biol. Lett.* **10**, 20140497. (doi:10.1098/rsbl.2014.0497)

11. Ribak G, Gish M, Weihs D, Inbar M. 2013 Adaptive aerial righting during the escape dropping of wingless pea aphids. *Curr. Biol.* **23**, R102–R103. (doi:10.1016/j.cub.2012.12.010)

12. Yanoviak SP, Munk Y, Kaspari M, Dudley R. 2010 Aerial manoeuvrability in wingless gliding ants (*Cephalotes atratus*). *Proc. R. Soc. B* **277**, 2199–2204. (doi:10.1098/rspb.2010.0170)

13. Dingle H. 1961 Flight and swimming reflexes in giant water bugs. *Biol. Bull* **121**, 117–128. (doi:10.2307/1539464)

14. Binns ES. 1977 Take-off and the 'tarsal reflex' in *Aphis fabae*. *Physiol. Entomol.* **2**, 97–102. (doi:10.1111/j.1365-3032.1977.tb00083.x)

15. Arbas EA. 1983 Aerial manoeuvring reflexes in flightless grasshoppers. *J. Exp. Biol.* **107**, 509–513.

16. Arbas EA. 1986 Control of hindlimb posture by wind-sensitive hairs and antennae during locust flight. *J. Comp. Physiol. A* **159**, 849–857. (doi:10.1007/BF00603738)

17. Yanoviak SP, Kaspari M, Dudley R. 2009 Gliding hexapods and the origins of insect aerial behaviour. *Biol. Lett.* **5**, 510–512. (doi:10.1098/rsbl.2009.0029)

18. Munk Y, Yanoviak SP, Koehl MA, Dudley R. 2015 The descent of ant: field-measured performance of gliding ants. *J. Exp. Biol.* **218**(Pt 9), 1393–1401. (doi:10.1242/jeb.106914)

19. Yanoviak SP, Munk Y, Dudley R. 2015 Arachnid aloft: directed aerial descent in neotropical canopy spiders. *J. R. Soc. Interface* **12**, 20150534. (doi:10.1098/rsif.2015.0534)

20. Zeng Y, Lin Y, Abundo A, Dudley R. 2015 Visual ecology of directed aerial descent in first-instar nymphs of the stick insect *Extatosoma tiaratum*. *J. Exp. Biol.* **218**, 2305–2314. (doi:10.1242/jeb.109553)

21. Schneider CA, Rasband WS, Eliceiri KW. 2012 NIH image to ImageJ: 25 years of image analysis. *Nat. Methods* **9**, 671–675. (doi:10.1038/nmeth.2089)

22. Walker JA. 1998 Estimating velocities and accelerations of animal locomotion: a simulation experiment comparing numerical differentiation algorithms. *J. Exp. Biol.* **201**, 981–995.

23. Team RC. 2013 *R: a language and environment for statistical computing*. Vienna, Austria: R Core Team.

24. Murray RM, Li Z, Sastry S. 1994 *A mathematical introduction to robotic manipulation*. Boca Raton, FL: CRC Press.

25. Jusufi A, Kawano DT, Libby T, Full RJ. 2010 Righting and turning in mid-air using appendage inertia: reptile tails, analytical models and bio-inspired robots. *Bioinspir. Biomim.* **5**, 045001. (doi:10.1088/1748-3182/5/4/045001)

26. Dudley R. 2000 *The biomechanics of insect flight: form, function, evolution*. Princeton, NJ: Princeton University Press.

27. Krämer K, Markl H. 1978 Flight-inhibition on ground contact in the American cockroach, *Periplaneta americana*— I. Contact receptors and a model for their central connections. *J. Insect Physiol.* **24**, 577–586. (doi:10.1016/0022-1910(78)90120-8)

28. Frantsevich L. 2004 Righting kinematics in beetles (Insecta: Coleoptera). *Arthropod. Struct. Dev.* **33**, 221–235. (doi:10.1016/j.asd.2004.05.007)

29. Kohlhage K, Yager J. 1994 An analysis of swimming in remipede crustaceans. *Phil. Trans. R. Soc. B* **346**, 213–221. (doi:10.1098/rstb.1994.0142)

30. Hustert R, Klug R. 2009 Evolution of a new sense for wind in flying phasmids? Afferents and interneurons. *Naturwissenschaften* **96**, 1411–1419. (doi:10.1007/s00114-009-0597-7)

31. Berthé R, Lehmann FO. 2014 Body appendages fine-tune posture and moments in freely manoeuvring fruit flies. *J. Exp. Biol.* **218**, 3295–3307. (doi:10.1242/jeb.122408)

32. Burrows M, Cullen DA, Dorosenko M, Sutton GP. 2015 Mantises exchange angular momentum between three rotating body parts to jump precisely to targets. *Curr. Biol.* **25**, 786–789. (doi:10.1016/j.cub.2015.01.054)

33. Hasenfuss I. 2002 A possible evolutionary pathway to insect flight starting from lepismatid organization. *J. Zoolog. Syst. Evol. Res.* **40**, 65–81. (doi:10.1046/j.1439-0469.2002.00180.x)

34. Dudley R, Byrnes G, Yanoviak SP, Borrell B, Brown RM, McGuire JA. 2007 Gliding and the functional origins of flight: biomechanical novelty or necessity? *Annu. Rev. Ecol. Evol.* **38**, 179–201. (doi:10.1146/annurev.ecolsys.37.091305.110014)

35. Bergou AJ, Swartz SM, Vejdani H, Riskin DK, Reimnitz L, Taubin G, Breuer KS. 2015 Falling with style: bats perform complex aerial rotations by adjusting wing inertia. *PLoS Biol.* **13**, 1002297. (doi:10.1371/journal.pbio.1002297)

36. Ma KY, Chirarattananon P, Fuller SB, Wood RJ. 2013 Controlled flight of a biologically inspired, insect-scale robot. *Science* **340**, 603–607. (doi:10.1126/science.1231806)

37. Hoover AM, Burden S, Fu X-Y, Sastry SS, Fearing RS. 2010 Bio-inspired design and dynamic maneuverability of a minimally actuated six-legged robot. Biomedical Robotics and Biomechatronics (BioRob). In *3rd IEEE RAS and EMBS Int. Conf., 26 September, The University of Tokyo, Tokyo, Japan*, pp. 869–876. Piscataway, NJ: IEEE.